Physica B 679 (2024) 415797

Contents lists available at ScienceDirect

Physica B: Condensed Matter

journal homepage: www.elsevier.com/locate/physb

Simultaneous effects of the position dependent mass and magnetic field on quantum well with the improved Tietz potential

Esin Kasapoglu [a], Melike Behiye Yücel [b], Carlos A. Duque [c], Miguel E. Mora-Ramos [d,*]

[a] Sivas Cumhuriyet University, Faculty of Science, Department of Physics, Sivas, 58140, Türkiye
[b] Akdeniz University, Faculty of Science, Department of Physics, Antalya, 07058, Türkiye
[c] Universidad de Antioquia UdeA, Grupo de Materia Condensada-UdeA, Instituto deFisica, Facultad de Ciencias Exactas y Naturales, Calle 70 No. 52-21, Medellin, 050010, Colombia
[d] Universidad Autónoma del Estado de Morelos, Centro de Investigación en Ciencias-IICBA, Av. Universidad 1001, Col.Chamilpa, Cuernavaca, 62209, Mexico

ARTICLE INFO

MSC:
35Q40
81V80
81V55-81V55
65C20
31C99

Keywords:
Improved Tietz potential
Morse potential
Rosen–Morse potential
Magnetic field
Position dependence mass

ABSTRACT

In this study, we explored the synergistic impact of position-dependent mass and magnetic field on the electronic and optical properties of quantum wells, featuring an enhanced Tietz potential confinement incorporating both standard Morse and improved Rosen–Morse potentials, as influenced by variations in the structural parameter. Calculations were conducted within the framework of effective mass and parabolic band approximations. The diagonalization method was employed, selecting a wave function basis of trigonometric orthonormal functions to determine the eigenvalues and eigenfunctions of the confined electron potential. Our findings reveal that alterations in the sizes and shapes of the quantum wells, magnetic field strength, geometric asymmetry, and confinement parameters lead to significant variations in electron energies, transition between electron states, and the absorption spectrum. These outcomes offer valuable insights for investigating the electronic and structural properties of materials and devising novel materials with tailored optical characteristics.

1. Introduction

As is well-known, the geometries of quantum well potentials have far-reaching implications in semiconductor physics and nanotechnology. Through meticulous engineering of these potentials, researchers can skillfully manipulate the behavior of confined particles, thereby creating innovative electronic, optical, and optoelectronic devices with tailored properties for diverse applications. The quantization of energy levels for particles within the structures is directly influenced by the geometry of the well, impacting the spacing and quantity of these energy levels. The adjustability of the dimensions of the quantum well holds substantial implications for the design of devices such as lasers, light-emitting diodes (LEDs) [1], and quantum cascade lasers [2], where specific energy transitions are indispensable for their optimal functionality. The width and depth of the quantum wells play a crucial role in determining the probability of tunneling, allowing particles to traverse through energy barriers that are classically forbidden. Such a property holds significant importance in the design of devices, such as tunneling and resonant tunneling diodes, which rely on the phenomenon of tunneling through thin barrier layers. The geometry of quantum wells plays a crucial role in determining the wavelength of emitted light. This particular effect is harnessed in optoelectronic devices like lasers and LEDs, where the recombination of electrons and holes leads to the emission of light.

The efficiency of light emission or absorption processes in optoelectronic devices hinges on the quantum efficiency, a factor influenced by the spatial overlap of the wave functions of confined particles. The geometry of the quantum wells directly impacts this spatial overlap, consequently influencing the efficiency of the device. In summary, the geometries of quantum well potentials have profound implications in semiconductor physics and nanotechnology. By meticulously engineering these potentials, researchers can manipulate the behavior of confined particles, paving the way for the creation of innovative electronic, optical, and optoelectronic devices with tailored properties for diverse applications.

By manipulating the parameters of low-dimensional semiconductor materials, including shape, size, width, and depth; the consideration of carrier-lattice interaction, and the application of external fields such as electric, magnetic, and intense laser fields, it is possible to finely tune the electronic, linear, and nonlinear optical properties of these materials based on specific objectives. The inherent characteristics of

* Corresponding author.
E-mail address: memora@uaem.mx (M.E. Mora-Ramos).

https://doi.org/10.1016/j.physb.2024.415797
Received 3 February 2024; Received in revised form 14 February 2024; Accepted 22 February 2024
Available online 24 February 2024
0921-4526/© 2024 Elsevier B.V. All rights reserved.

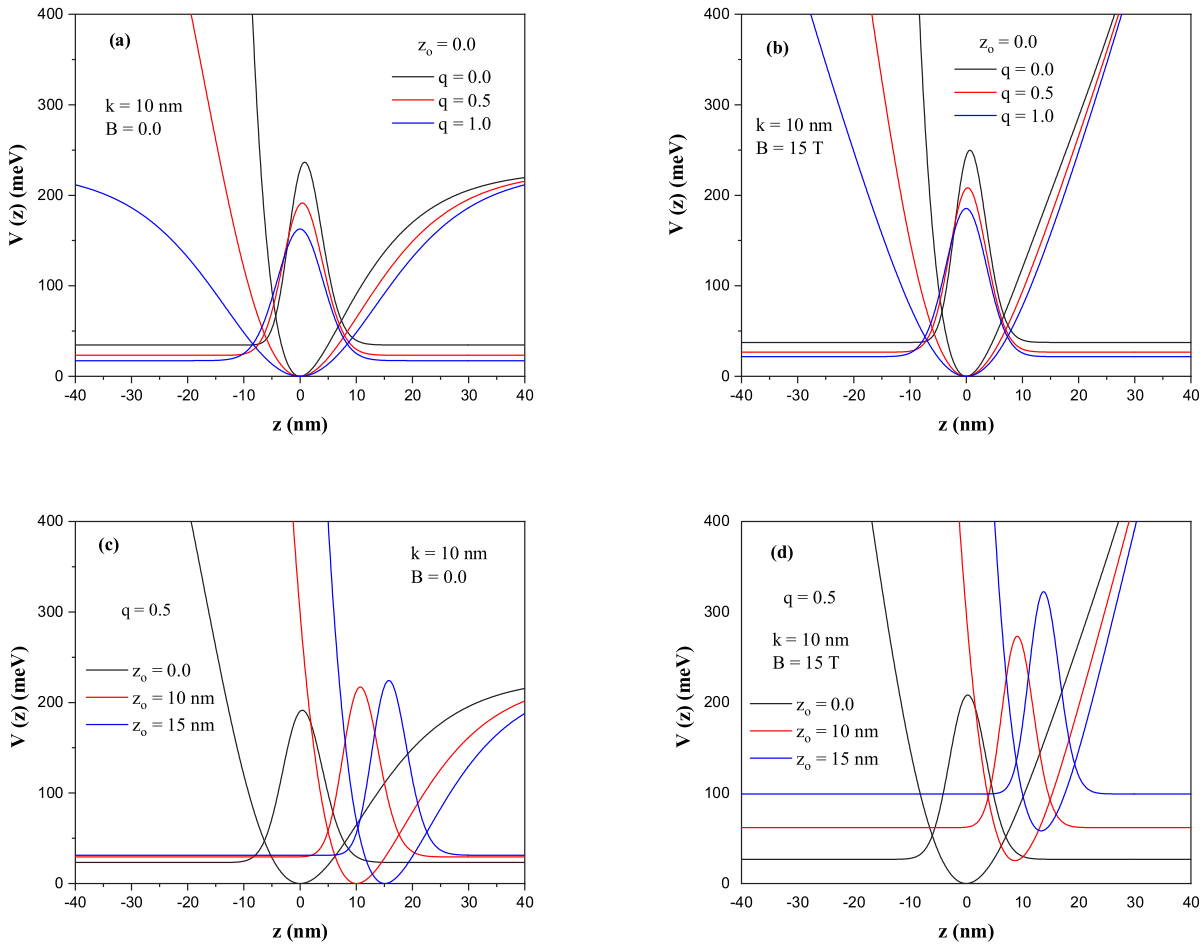


Fig. 1. For $k = 10$ nm, $z_0 = 0.0$, and different q-values, quantum well profiles and squared wave functions corresponding to the ground state of the electron localized within the well as a function of the z-growth direction coordinate: for $B = 0.0$ **(a)**, and $B = 15\ T$ **(b)**. For $k = 10$ nm, $q = 0.5$, and three different z_0-values, quantum well profiles and squared wave functions corresponding to the ground state of the electron localized within the well as a function of the z-growth direction coordinate: for $B = 0.0$ **(c)**, and $B = 15\ T$ **(d)**.

these materials make low-dimensional systems an ongoing focal point for both theoretical and experimental research [3–22].

In addition to the quantum well geometries traditionally use in modeling semiconductor heterostructures, in recent years, the electronic and optical properties of low-dimensional systems that have molecular potentials such as Konwent [23,24], Manning [25,26], Rosen–Morse [27,28], and Razavy [29] have been widely investigated either under the effects of external fields or under the effect of position-dependent mass (PDM). Model potentials of this class have been found to be reasonably accurate in comparison to experimental values of vibrational energies in diatomic molecules [30]. Their use in describing band bending in semiconductor quantum well structures has mostly to do with the actual non-abrupt shape of the confinement due to alloy diffusion, crystal growth inaccuracy, interface roughness, bond dissociation and vibrational behavior or, simply, with the increasing technological improvement that allows to design smooth variations of alloying to obtain desired confining profiles, as is the case of parabolic one in SiGe [31] and GaAs/AlGaAs [32] systems.

Numerous studies have explored the electronic and optical properties of semiconductors in the presence of position-dependent effective mass (PDM) and external fields. However, the combined effects of both PDM and external fields have received limited attention, with only one known Ref. [33]. In this cited work, nonlinear optical properties within GaAs/GaAlAs semi-parabolic and parabolic quantum wells were examined, considering constant effective mass (CM) and PDM, under various applied magnetic fields. This investigation serves as the primary motivation for our current study.

Our research delves into the concurrent impact of position-dependent mass and magnetic fields on the electronic and optical properties of potentials, specifically focusing on the improved Tietz potential [34,35]. This potential encompasses both Morse and improved Rosen–Morse potentials. To the best of our knowledge, a comprehensive study encompassing these aspects has not been previously undertaken.

2. Theory

In the effective mass approximation, the Hamiltonian for an electron under the magnetic field can be expressed as,

$$H = -\frac{\hbar^2}{2}\vec{\nabla}\cdot\left(\frac{1}{m(z)}\vec{\nabla}\right) + \frac{e^2B^2z^2}{2m(z)c^2} + V(z) \tag{1}$$

$m(z)$ is the effective mass of the electron as a function of position, and it is as defined below [36–42]

$$m(z) = m^* sech^2\left(\frac{\pi z}{d}\right) \tag{2}$$

where the d-parameter describes the effective length of PDM distribution, and $m^* = 0.067m_0$ is the effective mass of the electron in the GaAs material at $z = 0$ and m_0 is the free electron mass. At sufficiently large d-values, the variable mass approaches the value of electron mass in the bulk material of interest, and the uniform behavior, stability, and spatial extension of the effective mass also increase. The magnetic field-B is applied perpendicular to the z-growth direction, e is the elementary charge, and c is the speed of light. It should be noted that the vector potential to describe the applied magnetic field is written in the form of

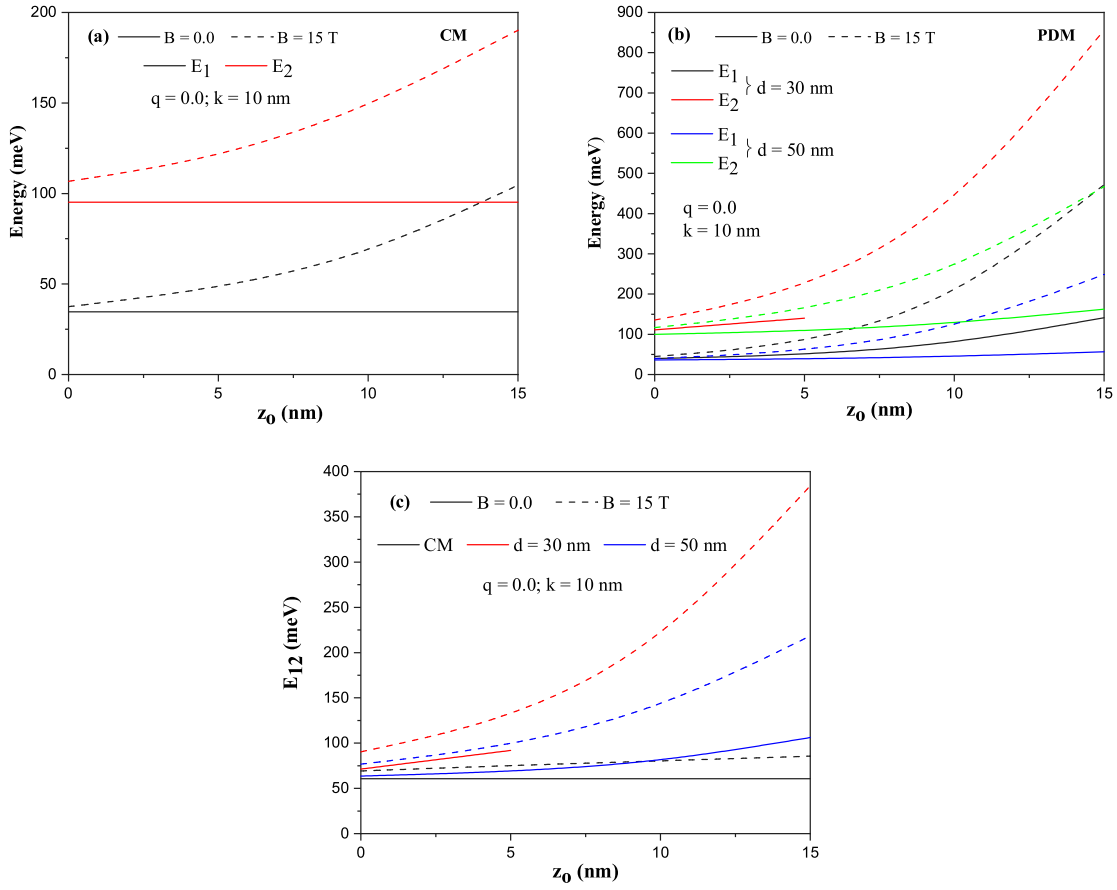


Fig. 2. $k = 10$ nm, the variation of the energies corresponding to the first two levels of the confined electron within the quantum well with the Morse confinement potential ($q = 0.0$) as a function of z_0-parameter in the cases of the constant mass **(a)**, and position dependence mass **(b)**, and the variations of the energy differences between the energy levels of interest energy levels as a function of z_0-parameter **(c)**. Solid lines (dashed lines) are for $B = 0.0$ ($B = 15$ T).

$\vec{A} = (0, -Bz, 0)$, and the improved Tietz potential energy function-$V(z)$ for diatomic molecules is given below [34,35]

$$V(z) = V_0 \left(1 - \frac{e^{z_0/k} + q}{e^{z/k} + q}\right)^2 \tag{3}$$

where V_0 is the depth of the quantum well, k-parameter is related to the well width, z_0 is the minimum point of the potential, it is also the distance from the equilibrium position, and also affects the well width. q is the adjustable parameter, when the parameter q has the values $0, +1$ and -1, the improved Tietz potential function turns into the standard Morse, improved Rosen–Morse, and improved Manning-Rosen potential functions, respectively. It should also be noted that this potential function which is used in the literature to obtain the molecular energy spectrum of diatomic molecules, has been modified by us to investigate the electronic and optical properties of an electron confined within this potential.

After obtaining the eigenvalues and eigenfunctions from the solution of Eq. (1) by the diagonalization method by selecting the orthonormal basis functions, which are the solutions of an infinite square quantum well, linear, third order nonlinear and total absorption coefficients (TACs) are found for transitions between any two electronic states by using the perturbation expansion and the density matrix methods [28,33,43], respectively

$$\beta^{(1)}(\omega) = \sqrt{\frac{\mu_0}{\varepsilon_r}} \frac{\left|M_{ij}\right|^2 \sigma_v \hbar\omega\Gamma_{ij}}{(E_{ij} - \hbar\omega)^2 + (\hbar\Gamma_{ij})^2}\,, \tag{4}$$

$$\beta^{(3)}(\omega, I) = -2\sqrt{\frac{\mu_0}{\varepsilon_r}} \left(\frac{I}{\varepsilon_0 n_r c}\right) \frac{\left|M_{ij}\right|^4 \sigma_v \hbar\omega\Gamma_{ij}}{\left[(E_{ij} - \hbar\omega)^2 + (\hbar\Gamma_{ij})^2\right]^2}$$

$$\times \left[1 - \frac{\left|M_{jj} - M_{ii}\right|^2}{\left|2M_{ij}\right|^2} \frac{(E_{ij} - \hbar\omega)^2 - (\hbar\Gamma_{ij})^2 + 2\, E_{ij}(E_{ij} - \hbar\omega)}{E_{ij}^2 + (\hbar\Gamma_{ij})^2}\right], \tag{5}$$

$$\beta(\omega, I) = \beta^{(1)}(\omega) + \beta^{(3)}(\omega, I)\,, \tag{6}$$

where, $\varepsilon_r = n_r^2 \varepsilon_0$ is the real part of the permittivity, σ_v is the carrier density in the system, μ_0 is the vacuum permeability, $E_{ij} = E_j - E_i$ is the energy difference between two impurity states, $M_{ij} = \left|\langle \psi_i | ez | \psi_j \rangle\right|$, $(i, j = 1, 2)$ is the transition matrix element between the eigenstates ψ_i and ψ_j for incident radiation polarized in the z-direction, Γ_{ij} $(= 1/T_{ij})$ is the relaxation rate, T_{ij} is the relaxation time, c is the speed of the light in free space, and I is the intensity of incident photon with the ω-angular frequency that leads to the intersubband optical transitions.

3. Results and discussions

The parameter values in our numerical calculations are, $m^* = 0.067 m_0$ (where m_0 is the free electron mass), $V_0 = 228$ meV, $\varepsilon = 12.58$, $n_r = \sqrt{\varepsilon} = 3.55$, $\varepsilon_0 = 8.85 \times 10^{-12}$ C^2 N^{-1} m^{-2}, $T_{12} = 0.4$ ps, $\Gamma_{12} = 1/T_{12}$, $\mu_0 = 4\pi \times 10^{-7}$ H m^{-1}, $\sigma_v = 3.0 \times 10^{22}$ m^{-3} and $I = 5.0 \times 10^8$ W/m^2. These parameters are suitable for GaAs/ GaAlAs heterostructures [13,44].

For $k = 10$ nm and $z_0 = 0.0$, various q-values are considered, and the quantum well profiles along with the squared wave functions corresponding to the ground state of the localized electron within the well are depicted in Fig. 1**(a)** and **(b)**, respectively. Similarly, when $k = 10$ nm and $q = 0.5$, Fig. 1**(c)** and **(d)** show the quantum well profiles and squared wave functions for the ground state in the absence and presence of a magnetic field.

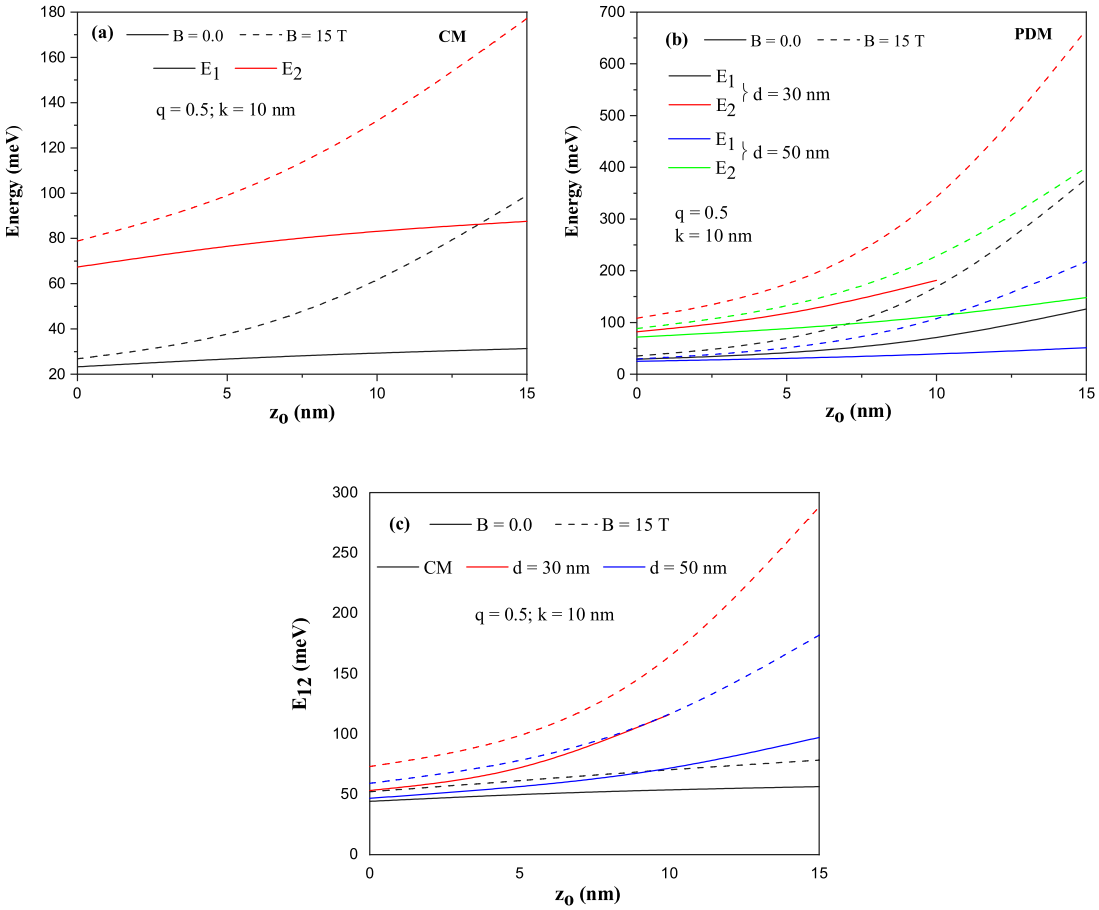


Fig. 3. $k = 10$ nm and ($q = 0.5$), the variation of the energies corresponding to the first two levels of the confined electron within the quantum well as a function of z_0-parameter in the cases of the constant mass **(a)**, and position dependence mass **(b)**, and the variations of the energy differences between the energy levels of interest energy levels as a function of z_0-parameter **(c)**. Solid lines (dashed lines) are for $B = 0.0$ ($B = 15$ T).

When $z_0 = 0.0$, the structure exhibits symmetrical characteristics; however, for nonzero z_0, it acquires an asymmetrical nature. Thus, we have defined z_0 as an asymmetry parameter. In such cases, the parameter z_0 significantly influences geometric confinement. As the value of z_0 increases, the minimum point of the potential shifts, and the barrier height on the right side gradually decreases, while the left side becomes sharper, rising towards infinity.

The magnetic field introduces an additional parabolic confinement on the quantum well due to the second term in Eq. (1). Consequently, the structure takes on an almost parabolic shape, with its minimum slowly shifting towards higher energies.

In Fig. 2, the variation of energies corresponding to the first two levels of a confined electron within a quantum well with the Morse confinement potential ($q = 0.0$) is depicted as a function of the z_0 parameter for both the CM **(a)** and PDM **(b)**. Additionally, the variations of transition energies between the specific levels are presented as a function of the z_0 parameter in **(c)**. Solid lines represent the case of $B = 0.0$, while dashed lines correspond to $B = 15$ T.

In the case of a CM without a magnetic field, the minimum point of the Morse potential shifts with increasing z_0 values; however, the energies and energy differences remain constant. On the contrary, in the presence of a magnetic field, energies become increasing functions of the z_0 parameter. As z_0 increases, the impact of the magnetic field on the energy values becomes more pronounced. The reason for this is the strengthening of spatial carrier confinement under magnetic field intensification, as noticed from Fig. 1. The increment in transition energy values, E_{12} has to do with the highest rate of increment associated with the first excited state in comparison the ground one.

For the PDM case, energies and energy differences are increasing functions of the parameter-z_0. Thus, for $d = 30$ nm and $z_0 > 5$ nm, E_2-energy state corresponds to the unbound state (bear in mind the particular well shape for $q = 0.0$). At sufficiently large values of d, energies and energy differences also approach to their values in the CM case because of the variable mass approaches the constant mass value of the electron in the relevant material, and eventually E_2-energy state becomes the bound state again.

Figs. 3**(a–c)** and 4**(a–c)** adhere to the same conventions as illustrated in Fig. 2**(a–c)**. However, these figures correspond to choosing $q = 0.5$ and $q = 1.0$ (improved Rosen–Morse potential), respectively. For both q values, the energies and energy differences exhibit an increasing trend with respect to z_0 in the cases of the CM and PDM. The decline in energies with increasing q values suggests a weakening of geometric confinement (with the E_2 energy state corresponding to the unbound state for $d = 30$ nm when $z_0 > 10$ nm). Consequently, in the presence of a magnetic field, a significant rise in energies is observed as z_0 increases, as evident in Fig. 1**(b)** and **(d)**. The combined impact of the magnetic field and the parameter z_0 results in a more substantial increase in geometric confinement compared to their individual effects. The magnetic field induces a further increase towards higher energy values, as the right-side barrier of all quantum wells rises sharply to infinity, mirroring the behavior on the left side.

In both the absence and presence of the magnetic field for the CM case, the variation of total ACs corresponding to the $(1 - 2)$ transition, as a function of incident photon energy, for different z_0 values and q values is illustrated in Fig. 5**(a)** and **(b)**, respectively. Solid, dashed, and dotted lines represent $q = 0.0$, $q = 0.5$, and $q = 1.0$, respectively.

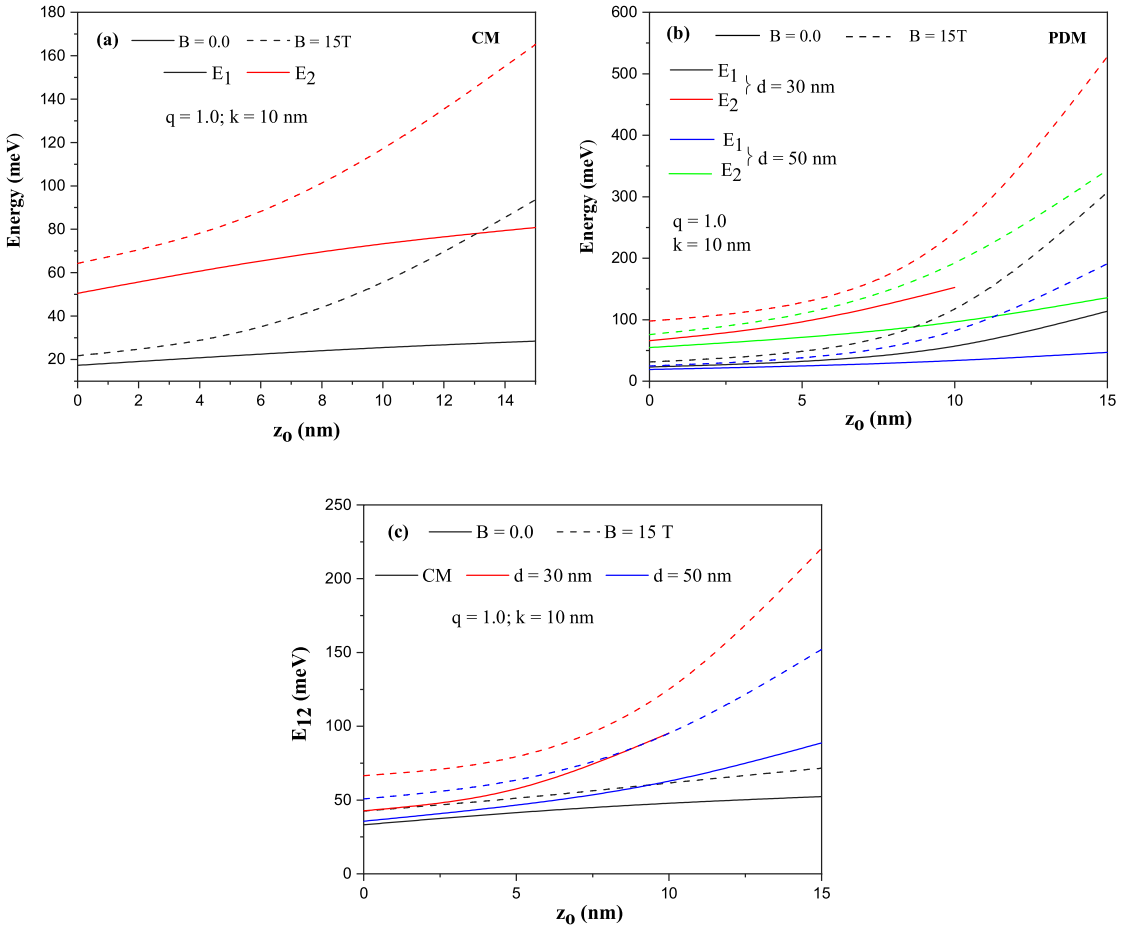


Fig. 4. k = 10 nm, the variation of the energies corresponding to the first two levels of the confined electron within the quantum well with improved Rosen–Morse potential (q = 1.0) as a function of z_0-parameter in the cases of the constant mass **(a)**, and position dependence mass **(b)**, and the variations of the energy differences between the energy levels of interest energy levels as a function of z_0-parameter **(c)**. Solid lines (dashed lines) are for $B = 0.0$ (B = 15 T).

It can be seen from the explanations in Fig. 2**(a)** and **(c)**, in the case of a CM without a magnetic field, regardless of the z_0 value, there is only a single absorption peak in the Morse potential (q = 0.0) since the energy does not change. At other q-values, absorption peaks shift towards lower photon energies with increasing z_0 values due to the weakening of the geometric confinement. In the presence of a magnetic field, there are absorption peaks belonging to the existing z_0 values for each q-value and a blue shift in the peak positions is observed, as well as the increase in peak amplitudes with increasing the magnetic field and z_0 values.

For the Morse potential (q = 0.0), the variation as a function of the incident photon energy of total ACs corresponding to the (1 – 2) transition -for different z_0-values- in the presence of the PDM appears in Fig. 6**(a)** and **(b)** for B = 0 and B = 15 T, respectively. As seen in Fig. 2**(b)** and **(c)**, for the z_0-values greater than 5 nm, the electronic states with E_2- energy within the QW unbound (unbound state corresponds to z_0 = 10 nm for the QW in the q = 0.0 case, and un-bound states correspond to z_0 = 15 nm for QWs in the q = 0.5 and q = 1.0 cases), and therefore the absorption peak is not observed for d = 30 nm, while it is observed for d = 50 nm. As z_0 increases, the peak positions shift to blue with increasing amplitude, and as the parameter-d increases, they shift to red with decreasing amplitude. Since the presence of the magnetic field causes an infinite parabolic confinement as seen in Fig. 1**(b)**, there is an absorption peak for each z_0-value and the absorption peaks shift towards quite large photon energies with increasing amplitudes.

The variation in total ACs corresponding to the (1 – 2) transition, as a function of the incident photon energy, for different z_0 values in the presence of the PDM for q = 0.5 and q = 1.0 (improved Rosen–Morse potential) are depicted in Figs. 7**(a–b)** and 8**(a–b)** for B = 0 and B = 15 T, respectively. In both the absence and presence of the magnetic field, the fluctuations in the positions and amplitudes of the absorption peaks mirror those in Fig. 6**(a)** and **(b)**, corresponding to q = 0.0. However, as illustrated in Figs. 7**(b)** and 8**(b)**, absorption peaks are not evident for z_0 = 15 nm and d = 30 nm, as there exists only one bound state at these confinement potentials. Conversely, for d = 50 nm, an absorption peak is observed due to the decrease in energy. Owing to the robust confinement induced by the magnetic field, the existence of any unbound electronic state is precluded. Consequently, an absorption peak is discernible for every combination of z_0 and d values under the influence of the magnetic field. It is noteworthy that with an increase in the q value, a red shift in the peak positions and a decrease in peak amplitudes are observed due to the attenuation of geometric confinement.

Altering the width of a quantum well fundamentally impacts the energy levels, quantum confinement effects, charge transport mechanisms, and the transition between localized and delocalized states of charge carriers. These events are significant in semiconductor devices like quantum wells used in lasers, quantum cascade lasers, and quantum computing devices. Understanding and manipulating the behavior of electrons between different confinement regions are crucial in designing and optimizing these devices [45].

To gain a clearer understanding of the impact of quantum well sizes on electronic and optical properties, our investigation was extended to k = 20 nm. In both the absence and presence of a magnetic field for the CM cases, the variations in total absorption coefficients corresponding

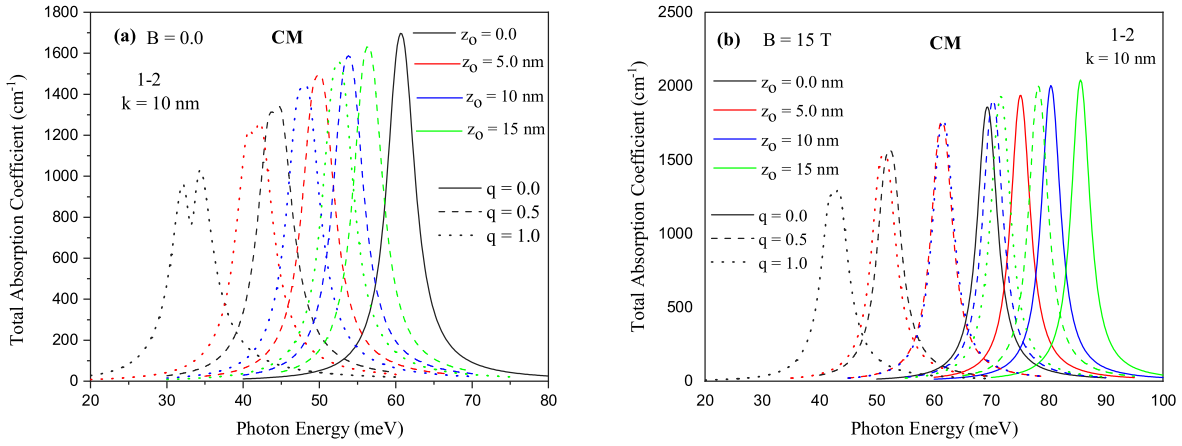


Fig. 5. For the case of the constant mass, the variation of total absorption coefficients corresponding to the (1 – 2) transition as a function of the incident photon energy for different z_0-values and q-values: **(a)** $B = 0.0$, and **(b)** $B = 15$ T. Solid, dashed and dotted lines are for $q = 0.0$, $q = 0.5$ and $q = 1.0$, respectively.

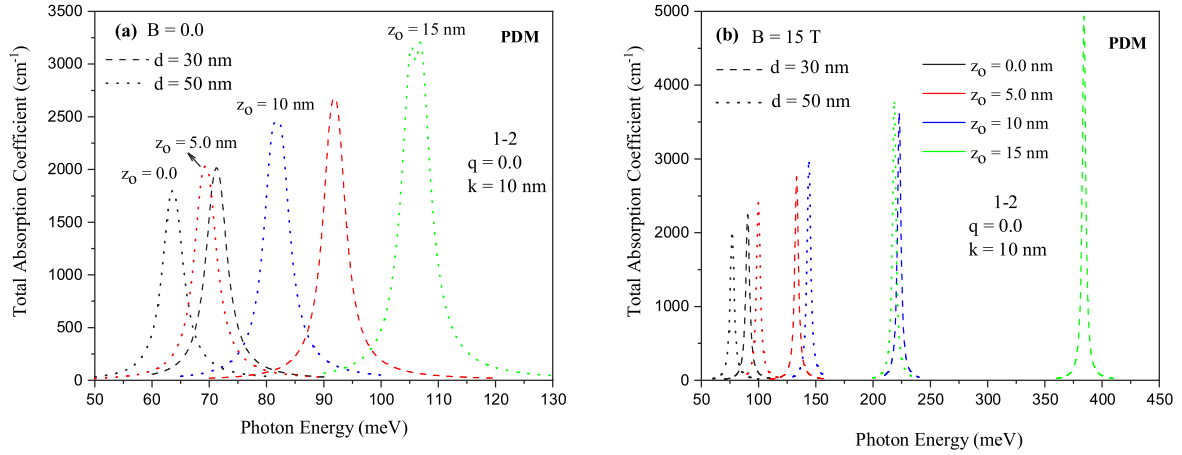


Fig. 6. For the Morse potential ($q = 0.0$), for the case of the position dependence mass the variation of total absorption coefficients corresponding to the (1 – 2) transition as a function of the incident photon energy for different z_0-values: **(a)** $B = 0.0$, and **(b)** $B = 15$ T. Dashed and dotted lines are for $d = 30$ nm and $d = 50$ nm, respectively.

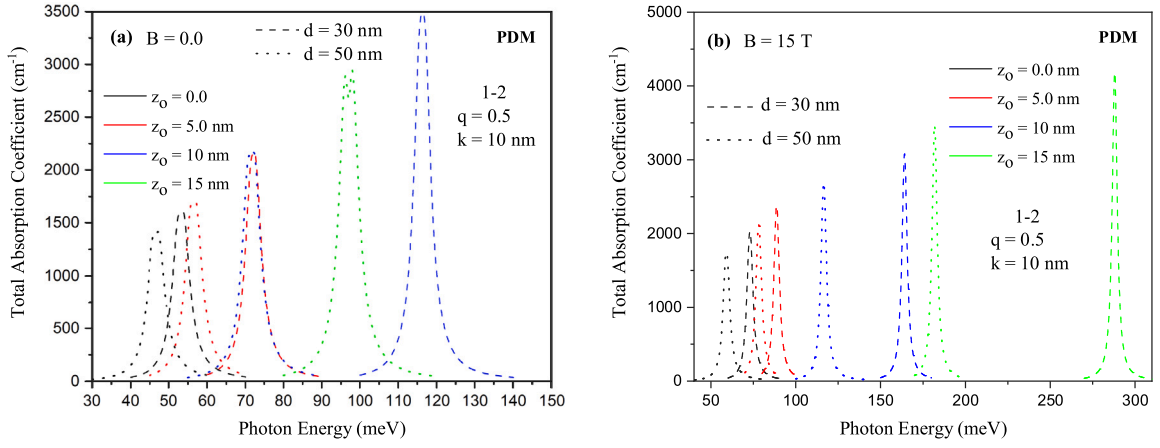


Fig. 7. For $q = 0.5$, for the case of the position dependence mass the variation of total absorption coefficients corresponding to the (1 – 2) transition as a function of the incident photon energy for different z_0-values: **(a)** $B = 0.0$, and **(b)** $B = 15$ T. Dashed and dotted lines are for $d = 30$ nm and $d = 50$ nm, respectively.

to the (1 – 2) transition were analyzed as a function of incident photon energy for different z_0-values and q-values, as illustrated in Fig. 9**(a)** and **(b)**, respectively. The figures depict solid, dashed, and dotted lines for $q = 0.0$, $q = 0.5$, and $q = 1.0$, respectively. It is well-established that an increase in well width weakens geometric confinement, leading to a decrease in electronic energies and the associated differences between them [44]. Consequently, absorption peak positions for the same z_0-values shift towards lower photon energies compared to the results obtained with $k = 10$ nm. Simultaneously, quantum effects diminish, causing the absorption spectrum to resemble that of a bulk material for larger well widths. As evident in these figures, the amplitudes of these peaks decrease with increasing values of k and q.

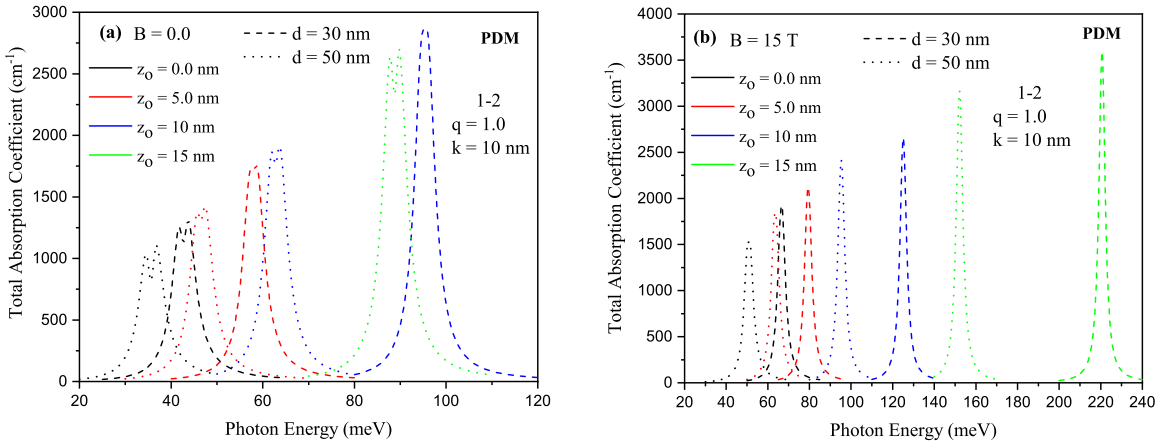


Fig. 8. For $q = 1.0$, in the case of the position dependence mass the variation of total absorption coefficients corresponding to the $(1-2)$ transition as a function of the incident photon energy for different z_0-values: **(a)** $B = 0.0$, and **(b)** $B = 15$ T. Dashed and dotted lines are for $d = 30$ nm and $d = 50$ nm, respectively.

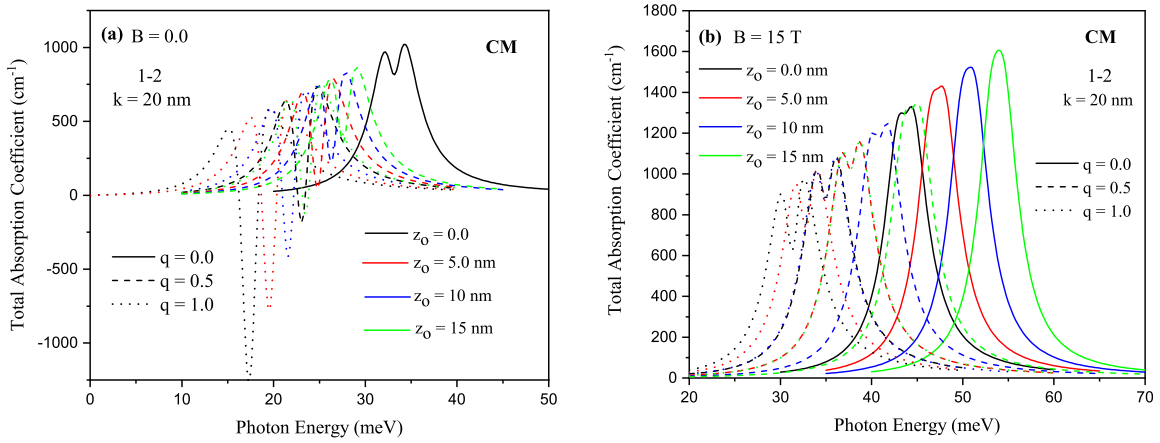


Fig. 9. For $k = 20$ nm and the constant mass case, the variation of total absorption coefficients corresponding to the $(1-2)$ transition as a function of the incident photon energy for different z_0-values and q-values for **(a)** $B = 0.0$, and **(b)** $B = 15$ T.

Furthermore, as the q-values increase, the bleaching effect becomes more pronounced. The alterations in the positions and amplitudes of the absorption peaks, influenced by both the magnetic field and the structure parameter q, are depicted in Fig. 5**(b)**. Specifically, there is a solitary absorption peak corresponding to the $q = 0.0$ value, as the energies remain constant for all z_0 values. The impact of the robust confinement induced by the magnetic field leads to a gradual reduction and eventual disappearance of the bleaching effects observed in the absence of the magnetic field, commencing from the smallest q-value.

With an increase in the well width, resulting in a narrowing of the space between energy levels, the light intensity required for the optical transitions remains significantly strong. Consequently, under such circumstances, the bleaching effect persists. Notably, when the energy difference between two levels is minimal, the bleaching effect ceases to be observed at lower light intensities, apart from alterations to the structural parameters or the application of external fields, as noted in previous research [44].

For $k = 20$ nm, $B = 0.0$, and the PDM case, the variations of total ACs corresponding to the $(1-2)$ transition as a function of the incident photon energy for different z_0-values are given in Fig. 10**(a–c)** for **(a)** $q = 0.0$, **(b)** $q = 0.5$ and **(c)** $q = 1.0$, respectively. Dashed and dotted lines are for $d = 30$ nm and $d = 50$ nm, respectively. Fig. 11**(a–c)** have the same regulations as in Fig. 10**(a–c)**, but these figures are for $B = 15$ T.

When $k = 20$ nm, $B = 0.0$, and within the PDM case, the variations of total ACs corresponding to the $(1-2)$ transition as a function of the incident photon energy for different z_0-values are given in Fig. 10**(a–c)** for **(a)** $q = 0.0$, **(b)** $q = 0.5$ and **(c)** $q = 1.0$, respectively. Dashed and dotted lines are for $d = 30$ nm and $d = 50$ nm, respectively. Fig. 11**(a–c)** have the same regulations as in Fig. 10**(a–c)**, but these figures are for $B = 15$ T.

As seen in Fig. 10**(a–c)**, while absorption peaks are observed at all z_0-values for $q = 1.0$ and $d = 30$ nm, the absorption peaks are not observed in the values of $q = 0.0$ and $q = 0.5$ for $z_0 = 15$ nm because there is only one bound state at these confinement potentials, but for $d = 50$ nm the absorption peak is observed due to the decrease in energy for all q–values. With the effect of the parabolic confinement created by the magnetic field, the absorption peaks for the $(1-2)$ transition corresponding to each q-value at all z_0-values are observed in Fig. 11**(a–c)**, respectively.

4. Conclusion

In this study, we have undertaken a pioneering examination of the simultaneous impacts of position-dependent mass and a magnetic field applied parallel to the growth direction of the considered structure on the electronic and optical properties of a quantum well. We have incorporated an improved Tietz potential, encompassing molecular potentials such as the standard Morse and improved Rosen–Morse potentials. To our knowledge, these potentials have not been previously employed for exploring the electronic and optical characteristics of low-dimensional systems, aside from their application in calculating rotational-vibration energies of selected diatomic molecules.

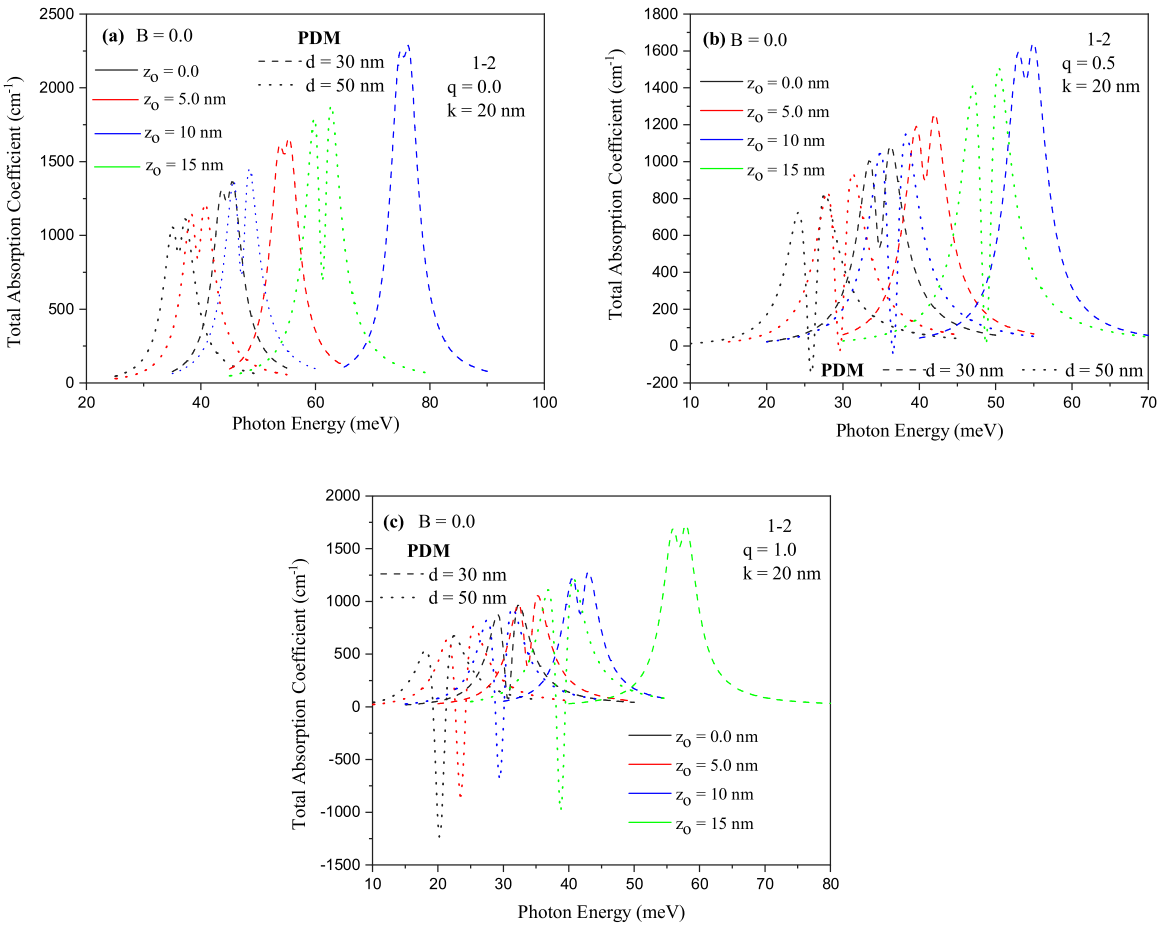


Fig. 10. For $k = 20$ nm, $B = 0.0$, and the position dependence mass case, the variations of total absorption coefficients corresponding to the $(1-2)$ transition as a function of the incident photon energy for different z_0-values: **(a)** $q = 0.0$, **(b)** $q = 0.5$ and **(c)** $q = 1.0$, respectively. Dashed and dotted lines are for $d = 30$ nm and $d = 50$ nm, respectively.

Our findings reveal that variations in the sizes and shapes of the quantum wells, magnetic field strength, asymmetry, and confinement parameters significantly influence the electronic and optical properties of these potentials. The observed blue shift in absorption peaks holds promise for practical applications in optoelectronics and photonics. By skillfully manipulating the blue shift, researchers could purposefully engineer the bandgap of low-dimensional materials, tailoring their optical and electronic attributes for specific device applications.

The phenomenon of a blue shift in absorption peaks holds considerable importance across diverse scientific and technological domains, including materials science, chemistry, and optics. It serves as a valuable tool for probing the electronic and structural aspects of materials, facilitating the development of new materials with customized optical properties. The chosen potentials in our study emerge as suitable tools for investigating both electronic and optical properties across various molecular and material systems. Besides, our results align qualitatively with certain studies of similar scope documented in the literature [44, 46].

So far, practical realization of these non-abrupt quantum well profiles in the GaAs/AlGaAs environment seems to have not been reported. However, technological possibilities with the use of molecular beam epitaxy would provide the scenario for such an achievement, as shown in Refs. [38,39] for the parabolic well system. We envisage that, similar to the latter and beyond their use as sources of nonlinear optical responses, the structures fabricated with an improved-Tietz-like potential could serve as a basis for THz emitters -when employing intersubband transitions- or as near-infrared emitters, based on interband transitions.

CRediT authorship contribution statement

Esin Kasapoglu: Writing – original draft, Formal analysis, Conceptualization. **Melike Behiye Yücel:** Validation, Software, Investigation. **Carlos A. Duque:** Writing – review & editing, Validation, Conceptualization. **Miguel E. Mora-Ramos:** Writing – review & editing, Writing – original draft, Validation.

Declaration of competing interest

The authors declare that they have no known competing financial interests or personal relationships that could have appeared to influence the work reported in this paper.

Data availability

Data will be made available on request.

Acknowledgments

MEMR acknowledges support from Mexican CONAHCYT through Grant CB 2017–2018 No. A1-S-8218. CAD is grateful to Colombian agencies CODI-Universidad de Antioquia (Estrategia de Sostenibilidad de la Universidad de Antioquia and projects “Propiedades magneto-ópticas *y* óptica no lineal en superredes de Grafeno”, “Estudio de propiedades ópticas en sistemas semiconductores de dimensiones nanoscópicas”, “Propiedades de transporte, espintrónicas *y* térmicas en el sistema molecular ZincPorfirina”, and “Complejos excitónicos

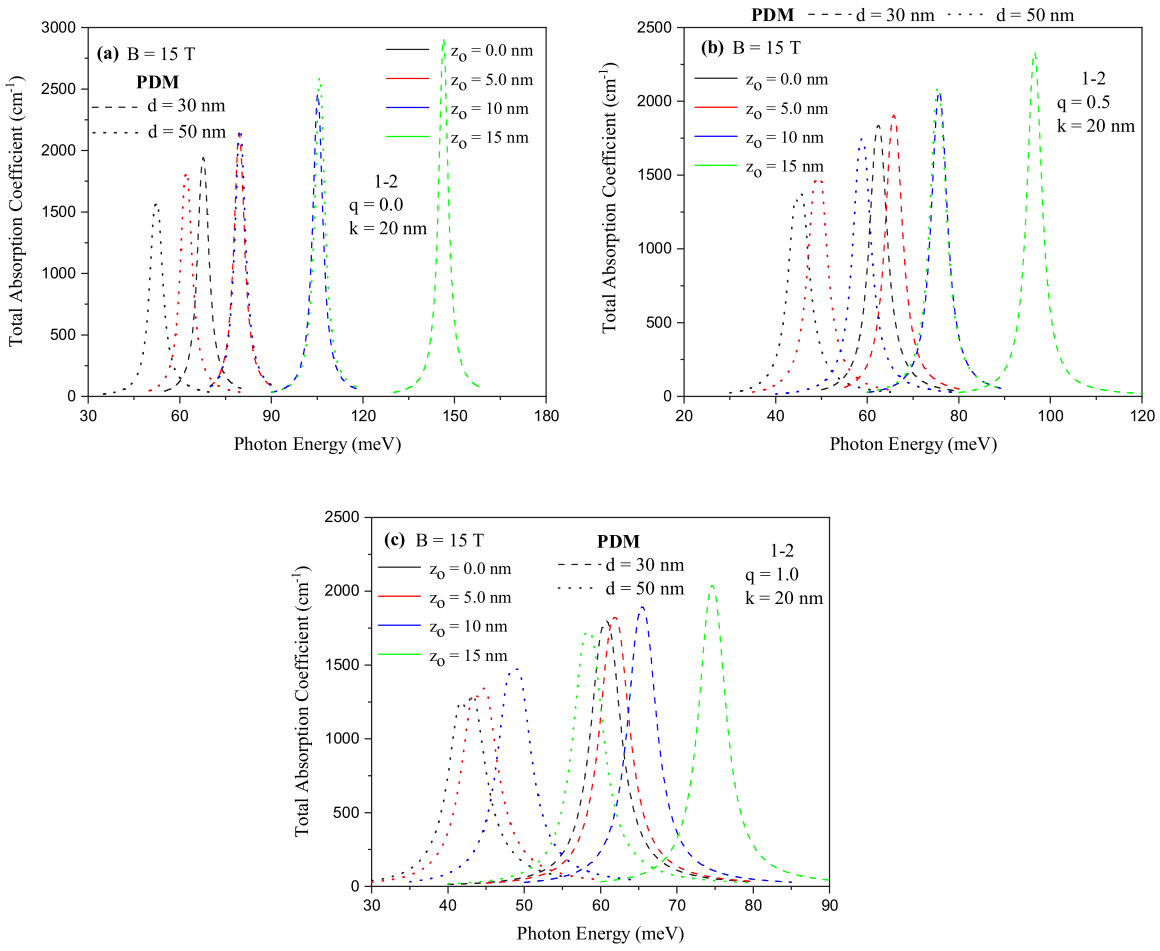


Fig. 11. For $k = 20$ nm, $B = 15$ T, and the position dependence mass case, the variations of total absorption coefficients corresponding to the $(1-2)$ transition as a function of the incident photon energy for different z_0-values: **(a)** $q = 0.0$, **(b)** $q = 0.5$ and **(c)** $q = 1.0$, respectively. Dashed and dotted lines are for $d = 30$ nm and $d = 50$ nm, respectively.

y propiedades de transporte en sistemas nanométricos de semiconductores con simetría axial") and Facultad de Ciencias Exactas *y* Naturales-Universidad de Antioquia (CAD exclusive dedication project 2022–2023). CAD also acknowledges the financial support from *El Patrimonio Autónomo Fondo Nacional de Financiamiento para la Ciencia*, la Tecnología *y* la Innovación Francisco José de Caldas (project: CD 111580863338, CT FP80740-173-2019).

References

[1] A.K. Viswanath, GaN nanostructure-based light emitting diodes and semiconductor lasers, J. Nanosci. Nanotechnol. 14 (2014) 1947–1982.
[2] M.S. Vitiello, G. Scalari, B. Williams, P. De Natale, Quantum cascade lasers: 20 years of challenges, Opt. Express 23 (2015) 5167–5182.
[3] G. Vignesh, P. Nithiananthi, Effect of confinement potential on exciton diamagnetism in the perspective of constituent carriers in a quantum well, J. Phys. Chem. Solids 114 (2018) 187–194.
[4] M.G. Barseghyan, A.A. Kirakosyan, Electronic states in a step quantum well in a magnetic field, Physica E 28 (2005) 471–481.
[5] J.A. Gil-Corrales, A.L. Morales, C.A. Duque, Self-consistent study of GaAs/AlGaAs quantum wells with modulated doping, Nanomaterials 13 (2023) 913.
[6] F. Barreto-Basave, M.E. Mora-Ramos, F. Ungan, I. Perez-Quintana, C.A. Duque, Fibonacci hyperbolic quantum wells: a model for two-level non-linear optical response, Opt. Quantum Electron. 55 (2023) 87.
[7] I. Karabulut, Ü. Atav, H. Şafak, M. Tomak, Linear and nonlinear intersubband optical absorptions in an asymmetric rectangular quantum well, Eur. Phys. J. B 55 (2007) 283–288.
[8] W. Xiao, X.J. Miao, Y. Sun, X.-J. Ma, J.-L. Xiao, Parabolic potential and temperature effects on the magnetopolaron in a RbCl asymmetrical semi-exponential quantum well, J. Low Temp. Phys. 210 (2022) 209–231.
[9] T.-J. Ou, R. An, W. Zhang, Y. Han, H.-R. Rastegar-Sedehi, X.-J. Ma, J.-L. Xiao, The Landau-level structure of a single polaron in a nanorod under a non-uniform magnetic field, Commun. Theor. Phys. 75 (2023) 095701.
[10] J. Cui, Y. Sun, Sh. Han, W. Zhang, R. An, X.-J. Ma, P.-F. Li, J.-L. Xiao, The parabolic-Gaussian potential and phonon effects on the polaron levels in alkali halogen ionic crystal quantum wells, Internat. J. Theoret. Phys. 62 (2023) 217.
[11] H. Sari, F. Ungan, E. Kasapoglu, S. Sakiroglu, I. Sökmen, Intense laser-induced electronic and optical properties in double finite oscillator potential, Phil. Mag. 99 (2019) 2444–2456.
[12] S. Baskoutas, C. Garoufalis, A.F. Terzis, Linear and nonlinear optical absorption coefficients in inverse parabolic quantum wells under static external electric field, Eur. Phys. J. B 84 (2011) 241–247.
[13] E. Kasapoglu, Binding energy of donor impurities in double inverse parabolic quantum well under electric field, Physica E 41 (2009) 1222–1225.
[14] C.A. Duque, M.E. Mora-Ramos, E. Kasapoglu, H. Sari, I. Sökmen, Combined effects of intense laser field and applied electric field on exciton states in GaAs quantum wells: Transition from the single to double quantum well, Phys. Status Solidi (B) 249 (2012) 118–127.
[15] E. Kasapoglu, I. Sökmen, Interband absorption and exciton binding energy in an inverse parabolic quantum well under the magnetic field, Phys. Lett. A 372 (2007) 56–59.
[16] E. Kasapoglu, F. Ungan, C.A. Duque, U. Yesilgul, M.E. Mora-Ramos, H. Sari, I. Sokmen, The effects of the electric and magnetic fields on the nonlinear optical properties in the step-like asymmetric quantum well, Physica E 61 (2014) 107–110.
[17] A. Keshavarz, M.J. Karimi, Linear and nonlinear intersubband optical absorption in symmetric double semi-parabolic quantum wells, Phys. Lett. A 374 (2010) 2675–2680.
[18] S. Baskoutas, C. Garoufalis, A.F. Terzis, Linear and nonlinear optical absorption coefficients in inverse parabolic quantum wells under static external electric field, Eur. Phys. J. B 84 (2011) 241–247.
[19] A. AL-Naghmaish, H. Dakhlaoui, T. Ghrib, B.M. Wong, Effects of magnetic, electric, and intense laser fields on the optical properties of AlGaAs/GaAs quantum wells for terahertz photodetectors, Physica B 635 (2022) 413838.
[20] H. Dakhlaoui, M. Nefzi, Tuning the linear and nonlinear optical properties in double and triple δ doped GaAs semiconductor: Impact of electric and magnetic field, Superlattices Microstruct. 136 (2019) 106292.

[21] N. Zeiri, N. Sfina, S. Abdi-BenNasrallah, M. Said, Linear and non-linear optical properties in symmetric and asymmetric double quantum wells, Optik 124 (2013) 7044–7048.
[22] N. Dinh Hien, Comparison of the nonlinear optical properties of asymmetrical and symmetrical quantum wells, Eur. Phys. J. B 95 (2022) 192.
[23] E.B. Al, E. Kasapoglu, S. Sakiroglu, H. Sari, I. Sökmen, Influence of position dependent effective mass on impurity binding energy and absorption in quantum wells with the Konwent potential, Mater. Sci. Semicond. Process. 135 (2021) 106076.
[24] K.A. Rodríguez-Magdaleno, F.M. Nava-Maldonado, E. Kasapoglu, M.E. Mora-Ramos, F. Ungan, J.C. Martínez-Orozco, Nonlinear absorption coefficient and relative refractive index change for Konwent potential quantum well as a function of intense laser field effect, Physica E 148 (2023) 115618.
[25] E. Kasapoglu, C.A. Duque, Position dependent effective mass effect on the quantum wells with three-parameter modified Manning potential, Optik 243 (2021) 166840.
[26] H. Dakhlaoui, W. Belhadj, E. Kasapoglu, F. Ungan, Position-dependent-mass and laser field impact on the optical characteristics of Manning-like double quantum well, Physica E 151 (2023) 115737.
[27] A. Salman Durmuslar, A. Turkoglu, M.E. Mora-Ramos, F. Ungan, The non-resonant intense laser field effects on the binding energies and the nonlinear optical properties of a donor impurity in Rosen–Morse quantum well, Indian J. Phys. 96 (2022) 3485–3492.
[28] E. Kasapoglu, M.B. Yücel, C.A. Duque, Position-dependent effective mass and asymmetry effects on the electronic and optical properties of quantum wells with improved Rosen–Morse potential, Condens. Matter 86 (2023) 1–12.
[29] E. Kasapoglu, H. Sari, I. Sökmen, J.A. Vinasco, D. Laroze, C.A. Duque, Effects of intense laser field and position dependent effective mass in Razavy quantum wells and quantum dots, Physica E 126 (2021) 114461.
[30] R.K. Pingak, A.Z. Johannes, Z.S. Ngara, M. Bukit, F. Nitti, D. Tambaru, M.Z. Ndii, Accuracy of Morse and Morse-like oscillators for diatomic molecular interaction: A comparative study, Results Chem. 3 (2021) 100204.
[31] M. Montanari, C. Ciano, L. Persichetti, C. Corley, L. Baldassarre, M. Ortolani, L. DiGaspare, G. Capellini, D. Stark, G. Scalari, M. Virgilio, M. DeSeta, Thz intersubband absorption in n-type $Si_{1-x}Ge_x$ parabolic quantum wells, Appl. Phys. Lett. 118 (2021) 163106.
[32] M. Karaliūnas, E. Dudutienė, A. Čerškus, J. Pagalys, S. Pūkienė, A. Udal, R. Butkutė, G. Valušis, High precision parabolic quantum wells grown using pulsed analog alloy grading technique: Photoluminescence probing and fractional-dimensional space approach, J. Lumin. 239 (2021) (2021) 118321.
[33] Z.H. Zhang, K.X. Guo, J.H. Yuan, Influence of the position dependent effective mass on the nonlinear optical properties in semiparabolic and parabolic quantum well with applied magnetic field, Physica E 108 (2019) 238–243.
[34] C.S. Jia, C.W. Wang, L.H. Zhang, X.L. Peng, R. Zeng, X.T. You, Partition function of improved Tietz oscillators, Chem. Phys. Lett. 676 (2017) 150–153.
[35] C.S. Jia, Y.F. Diao, X.J. Liu, P.Q. Wang, J.Y. Liu, G.D. Zhang, Equivalence of the Wei potential model and Tietz potential model for diatomic molecules, J. Chem. Phys. 137 (2012) 014101.
[36] H. Sari, E. Kasapoglu, S. Sakiroglu, I. Sokmen, Position-dependent mass effects on the optical responses of the quantum well with Tietz–Hua potential, Optik 178 (2019) 1280–1284.
[37] H. Panahi, S. Golshani, M. Doostdar, Influence of position dependent effective mass on donor binding energy in square and V-shaped quantum wells in the presence of a magnetic field, Physica B 418 (2013) 47–51.
[38] A. Khlevniuk, V. Tymchyshyn, Classical treatment of particle with position-dependent mass m(r) = 1/(1 + r4) in 1D and 2D subjected to harmonic potential, J. Math. Phys. 59 (2018) 082901.
[39] A. John Peter, K. Navaneethakrishnan, Effects of position-dependent effective mass and dielectric function of a hydrogenic donor in a quantum dot, Physica E 40 (2008) 2747–2751.
[40] A. John Peter, The effect of position dependent effective mass of hydrogenic impurities in parabolic GaAs/GaAlAs quantum dots in a strong magnetic field, Internat. J. Modern Phys. B 23 (2009) 5109–5118.
[41] R.M. Lima, H.R. Christiansen, The kinetic Hamiltonian with position-dependent mass, Physica E 150 (2023) 115688.
[42] I. Maouhoubi, R. En-nadir, S. Maouhoubi, I. Zorkani, A.O.T. Hassani, A. Jorio, The effects of lateral electric field, effective-mass position-dependent, and dimension on the donor-impurity binding energy and electron–impurity distance in GaAs-based quantum disk, Physica E 148 (2023) 115630.
[43] R. En-nadir, H. El-ghazia, W. Belaid, M. Tihtih, H. Abboudi, I. Maouhoubi, J. Anouar, I. Zorkani, Intrasubband-related linear and nonlinear optical absorption in single, double and triple QW: the compositions, temperature and QW's number effects, Phil. Mag. 103 (2023) 547–560.
[44] E. Kasapoglu, M.B. Yücel, C.A. Duque, Electronic and optical properties of the exponential and hyperbolic Rosen–Morse types quantum wells under applied magnetic field, Eur. Phys. J. Plus 138 (2023) 1026.
[45] J. Dong, C. Wu, Crossover from hopping to band-like transport in crystalline organic semiconductors: The effect of shallow traps, J. Chem. Phys. 150 (2019) 044903.
[46] Z.H. Zhang, J.H. Yuan, K.X. Guo, The combined influence of hydrostatic pressure and temperature on nonlinear optical properties of GaAs/Ga0.7Al0.3As morse quantum well in the presence of an applied magnetic field, Materials 11 (5) (2018) 668.